Spectrally Robust Photon-Pair Generation in Topological Waveguide Arrays

A. Zecchetto,[1] J.-R. Coudevylle,[2] M. Morassi,[2] A. Lemaître,[2] M. I. Amanti,[1] S. Ducci,[1] and F. Baboux[1,3,*]

[1]*Université Paris Cité, CNRS, Laboratoire Matériaux et Phénomènes Quantiques, 75013 Paris, France*

[2]*Université Paris-Saclay, CNRS, Centre de Nanosciences et de Nanotechnologies, 91120 Palaiseau, France*

[3]*Institut Universitaire de France (IUF)*

(Received 23 March 2026; revised 17 July 2026; accepted 17 September 2026; published 12 November 2026)

Harnessing topological effects offers a route to protect quantum states of light from imperfections, potentially enabling more robust platforms for quantum information processing. This capability is particularly relevant for active photonic circuits that generate quantum light directly on-chip. However, the impact of topology on the spectral properties of parametric processes—crucial for scalable quantum photonic circuits—remains largely unexplored. Here, we address this question by investigating photon-pair generation via spontaneous parametric down-conversion (SPDC) in nonlinear waveguide arrays, combining experiment and theory. A systematic comparison of uniform, trivial, and topological Su-Schrieffer-Heeger (SSH) arrays reveals that only the topological configuration preserves a stable SPDC resonance spectrum under coupling disorder, with fluctuations in the resonance wavelength reduced by more than an order of magnitude. An analytical model captures the origin of this robustness in the band-structure properties of the interacting modes. Numerical analysis further shows that each SSH array can operate as a robust photon-pair source, enabling stable interference between multiple such sources and the generation of high-dimensional entangled states with high fidelity. These results establish nonlinear waveguide arrays as a promising platform for harnessing the interplay of topology and nonlinearity in quantum photonic circuits.

DOI: 10.1103/kszt-p63d

I. INTRODUCTION

Integrated photonic circuits have emerged as a powerful platform for generating and manipulating complex quantum states of light in compact and scalable architectures [1]. Among the various implementations, continuously coupled systems such as waveguide arrays are attracting growing interest for quantum information applications [2–17]. In these structures, photons are continuously transferred between neighboring waveguides through evanescent coupling as they propagate. This enables distributed interference along the full propagation length and gives rise to rich band-structure physics that can be described by lattice Hamiltonians [18]. This intrinsic connection to condensed-matter models has enabled optical simulations of Anderson localization [19], Bloch oscillations [20], quantum transport [21,22], and topological phenomena [23–25].

In particular, topological photonic lattices have recently enabled controlled manipulation of quantum states of light in integrated platforms. Experiments in passive glass circuits, where quantum states are injected externally, have demonstrated quantum interference of topological single-photon states [8], the robustness of second-order cross-correlation functions in quasi-periodic lattices [26], or the protection of polarization-entangled states against disorder in Su-Schrieffer-Heeger (SSH) arrays [27].

In active platforms, where quantum light is generated directly on chip via optical nonlinearities [28–30], topological effects have also provided tangible benefits. In silicon-based waveguide arrays exploiting $\chi^{(3)}$ nonlinearity, squeezed states supported by SSH modes have been realized [31], albeit without probing the effect of disorder. The topological protection of the spatial profile of biphoton states against disorder, on the other hand, has been convincingly demonstrated in [9,32,33], further confirming the practical relevance of this approach.

However, these demonstrations primarily concern spatial-mode properties of quantum states. The protection of *spectral* features of quantum light generation [34], such as the resonance spectrum of the underlying nonlinear interaction or the emission spectrum of photon pairs, has not yet been established in waveguide-array platforms.

*Contact author: florent.baboux@u-paris.fr

Published by the American Physical Society under the terms of the Creative Commons Attribution 4.0 International license. Further distribution of this work must maintain attribution to the author(s) and the published article's title, journal citation, and DOI.

These features are nevertheless essential for complex photonic circuits, where multiple parametric sources generate quantum states that must subsequently interfere within the circuit [35–37]. Since these sources are typically pumped by a single laser beam that is split among them, it is important that despite inevitable fabrication imperfections, they all exhibit the same resonance wavelength (with minimal uncertainty), and that they produce photon pairs or heralded single photons with identical emission spectra. Achieving such spectral uniformity—a prerequisite for high-visibility quantum interference in complex circuits—raises the question of whether topological protection can be extended to the spectral features of quantum light generation in waveguide arrays.

Here, we address this question theoretically and experimentally by focusing on the resonance spectrum of spontaneous parametric down-conversion (SPDC) in $\chi^{(2)}$ waveguide arrays. We systematically compare different lattice geometries: uniform arrays, arrays featuring a trivial localized mode, and topological SSH arrays in the presence of coupling disorder. While disorder strongly affects the SPDC resonance spectrum in the first two cases, inducing significant fluctuations in both its shape and peak position, the resonance spectrum of topological arrays remains robust up to substantial disorder levels. Our experiments carried out in AlGaAs waveguide arrays, chosen for their strong $\chi^{(2)}$ nonlinearity enabling efficient on-chip SPDC, are supported by exact numerical simulations and an analytical model that captures these different behaviors and traces them back to the band-structure properties of the interacting modes. To our knowledge, these results provide the first experimental demonstration of topological protection of the resonance spectrum of quantum light generation in a one-dimensional system, paving the way for simple and compact on-chip implementations. A systematic numerical analysis further indicates that this spectral robustness translates into enhanced stability of the generated biphoton properties, including greater resilience to fabrication imperfections than conventional single-waveguide sources. Each SSH array can therefore act as a robust photon-pair source, allowing stable interference between multiple such sources even in the presence of disorder, opening perspectives for scalable quantum information processing and simulation on-chip.

II. THEORETICAL FRAMEWORK

We consider an array of $\chi^{(2)}$ nonlinear waveguides with coupling constants $C_{n,n+1}$ between neighboring waveguides. A monochromatic pump beam at frequency ω_p (shown in red in Fig. 1) propagates along the array and continuously generates signal and idler photons (frequencies ω_s and ω_i) by SPDC, which subsequently undergo quantum walks (as sketched in blue) through evanescent

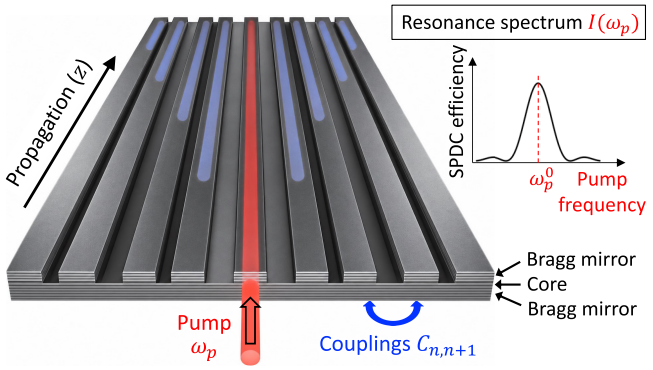


FIG. 1. Working principle of a $\chi^{(2)}$ nonlinear waveguide array (here implementing the Su-Schrieffer-Heeger model). A monochromatic pump beam at frequency ω_p (sketched in red) is injected into the central waveguide, generating pairs of signal and idler photons through spontaneous parametric down-conversion. These photons can couple evanescently between adjacent waveguides (as sketched in blue), with coupling constants $C_{n,n+1}$. The resonance spectrum (inset) quantifies the efficiency of photon-pair generation as a function of the pump frequency and serves here as a figure of merit to probe the stability of the SPDC process against disorder.

coupling between adjacent waveguides. We assume co-polarized, spectrally degenerate photons, $\omega_s = \omega_i = \omega_p/2$, such that the signal and idler share identical propagation and coupling constants. The biphoton state at the array output can be written as $|\Psi\rangle = \sum_{n_s,n_i} \Psi_{n_s,n_i} |n_s, n_i\rangle$, where Ψ_{n_s,n_i} governs the probability amplitude to detect one photon in waveguide n_s and the other in n_i. It obeys coupled-mode equations along the propagation direction z [38,39]:

$$\frac{d\Psi_{n_s,n_i}}{dz} = i\,\mathcal{C}[\Psi] + \gamma\,\delta_{n_s,n_i}\,A_{n_s}(z)e^{i\Delta\beta^{(0)}_{n_s} z}, \tag{1}$$

where $\mathcal{C}[\Psi]$ denotes, for compactness, the nearest-neighbor coupling terms [40], γ quantifies the SPDC efficiency, and the Kronecker delta δ_{n_s,n_i} enforces that the signal and idler photons are generated in the same waveguide $n_s = n_i \equiv n$. Here, $A_n(z)$ is the pump amplitude in waveguide n, and $\Delta\beta^{(0)}_n = \beta^p_n - \beta^s_n - \beta^i_n$ is the single-waveguide phase mismatch, where β^p_n, β^s_n, and β^i_n are the propagation constants of the pump, signal, and idler fields in waveguide n. The pump field follows analogous coupled-mode equations with reduced coupling constants $C^p_{n,n+1} = \alpha\, C_{n,n+1}$, with $\alpha \ll 1$ since the coupling of the pump is much less efficient due to its halved wavelength [4]. Full equations are provided in Supplemental Material [40].

We inject the pump into the central waveguide (labeled $n = 0$) and investigate the SPDC resonance spectrum, which quantifies the photon-pair generation efficiency as a function of the pump frequency. We evaluate this spectrum at the output of the central waveguide as

$I(\omega_p) = |\Psi_{0,0}(z = L)|^2$, where L is the array length. Experimentally, this corresponds to coincidence counts recorded while scanning the pump frequency (see inset of Fig. 1).

We first consider a uniform periodic array, with identical coupling constants $C_{n,n+1} = C$ for all n, as sketched in Fig. 2(a) (cross-section view). Figure 2(c) shows (black bold line) the calculated resonance spectrum of an array of 13 waveguides, using realistic parameters that will be explored experimentally below (see caption for details), with a pump wavelength around 775 nm generating photon pairs in the telecom range. Since the simplified model of Eq. (1) assumes spectrally degenerate signal and idler photons, no spectral integration is involved in the simulations of Fig. 2. In contrast to a single waveguide, which would exhibit a sinc^2 resonance profile, the spectrum displays an enlarged and richer structure. Indeed, inter-waveguide coupling gives rise to a band structure for the propagation constants of both pump and SPDC fields, as illustrated in Fig. 2(b) in the infinite-lattice limit. The corresponding discrete supermodes of the finite array enable multiple phase-matching channels, producing the observed broad and structured resonance spectrum [38,39,40].

We next introduce disorder in the coupling constants to model fabrication imperfections. We assume a uniform distribution of relative amplitude Δ, such that $C_{n,n+1} \in [C(1-\Delta), C(1+\Delta)]$ (which translates to the pump according to $C^p_{n,n+1} = \alpha\, C_{n,n+1}$), and we compute the resonance spectrum for different realizations of disorder $\Delta = 40\%$, as shown with thin colored lines in Fig. 2(c). The spectra are normalized by their area for clarity. They exhibit strong fluctuations, both in their overall shape and in the position of the resonance peak, marked by dots. To quantify these variations, we analyze 1000 disorder realizations at each disorder strength and compute the spectral overlap of each resonance spectrum with the disorder-free spectrum, as a measure of spectral stability. Figure 2(d) reports the median spectral overlap and its spread (error bars indicate the variability across realizations). As disorder increases, the median overlap decreases rapidly, while its spread grows. Figure 2(e) further shows that the standard deviation of the resonance-peak position increases monotonically with disorder. Together, these results demonstrate the strong sensitivity of both the resonance shape and the peak position to disorder in uniform waveguide arrays.

We next consider an SSH array, obtained by alternating short and long spacings between adjacent waveguides [43]. A topological interface is introduced at the center by inserting an additional long spacing, as sketched in Fig. 2(k). This gives rise to a topological mode exponentially localized on the central waveguide (blue), which resides at the center of the band structure [horizontal dotted line in Fig. 2(l)] [44]. Its propagation constant is protected against coupling disorder by chiral symmetry, and isolated from the bulk spectrum by a band gap of width $4KC$ (in the infinite-lattice limit), where K is the dimerization parameter controlling the modulation of the couplings [45,46]. Using the same parameters as in Fig. 2(c), Fig. 2(m) displays the calculated resonance spectra for $K = 0.5$, without disorder (bold black line) and for various disorder realizations (thin colored lines) with $\Delta = 40\%$. In strong contrast with the uniform array case, the spectra are nearly identical and exhibit a symmetric, single-peak profile. Figures 2(n) and 2(o) show the statistics of the spectral overlap and of the resonance-peak position as a function of disorder strength. The spectral overlap remains close to unity, while fluctuations in the resonance-peak position are strongly suppressed compared to the uniform-array case. This spectral stability persists up to disorder strengths of $\Delta \approx 50\%$ (corresponding to the dimerization parameter K), around which a gradual crossover toward a more disorder-sensitive regime occurs.

One may question whether this robustness stems from lattice topology itself or simply from spatial localization of the interacting modes, which suppresses transverse propagation in the array and could thereby mitigate the impact of disorder on SPDC generation. To address this question, we consider a periodic array, albeit with a slightly wider central waveguide, as sketched in Fig. 2(f) (hereafter referred to as the "trivial-mode array"). The increased modal index at the center induces a spatially localized mode with an eigenvalue lying above the bulk band [Fig. 2(g)]. This mode is topologically trivial, and its propagation constant is not protected against disorder [44,46]. Figure 2(h) shows the corresponding resonance spectra without disorder (bold black line) and for various realizations of coupling disorder (thin colored lines) with $\Delta = 40\%$. While the spectrum remains single-peaked, with a shape comparable to that of the topological array, the peak position fluctuates strongly with disorder [Fig. 2(j)], leading to a rapid degradation of the spectral overlap as disorder increases [Fig. 2(i)]. This comparison demonstrates that spatial localization alone is insufficient to ensure robustness of the parametric resonance against disorder, highlighting the protective role of the SSH topology.

To complement the numerical simulations and elucidate the origin of these contrasting behaviors, we now introduce a simple analytical model capturing the essential physics. We express the biphoton state in the basis of spatial supermodes (lattice eigenmodes) as

$$|\Psi\rangle = \sum_j A_{m_p} \gamma_j\, L\, e^{i\Delta\beta_j L/2}\, \mathrm{sinc}(\Delta\beta_j L/2)\, \hat{a}^\dagger_{m_s} \hat{a}^\dagger_{m_i} |0\rangle, \quad (2)$$

where the sum runs over all combinations of pump, signal, and idler supermodes, $j = \{m_p, m_s, m_i\}$. Here, $\hat{a}^\dagger_{m_s}$ ($\hat{a}^\dagger_{m_i}$)

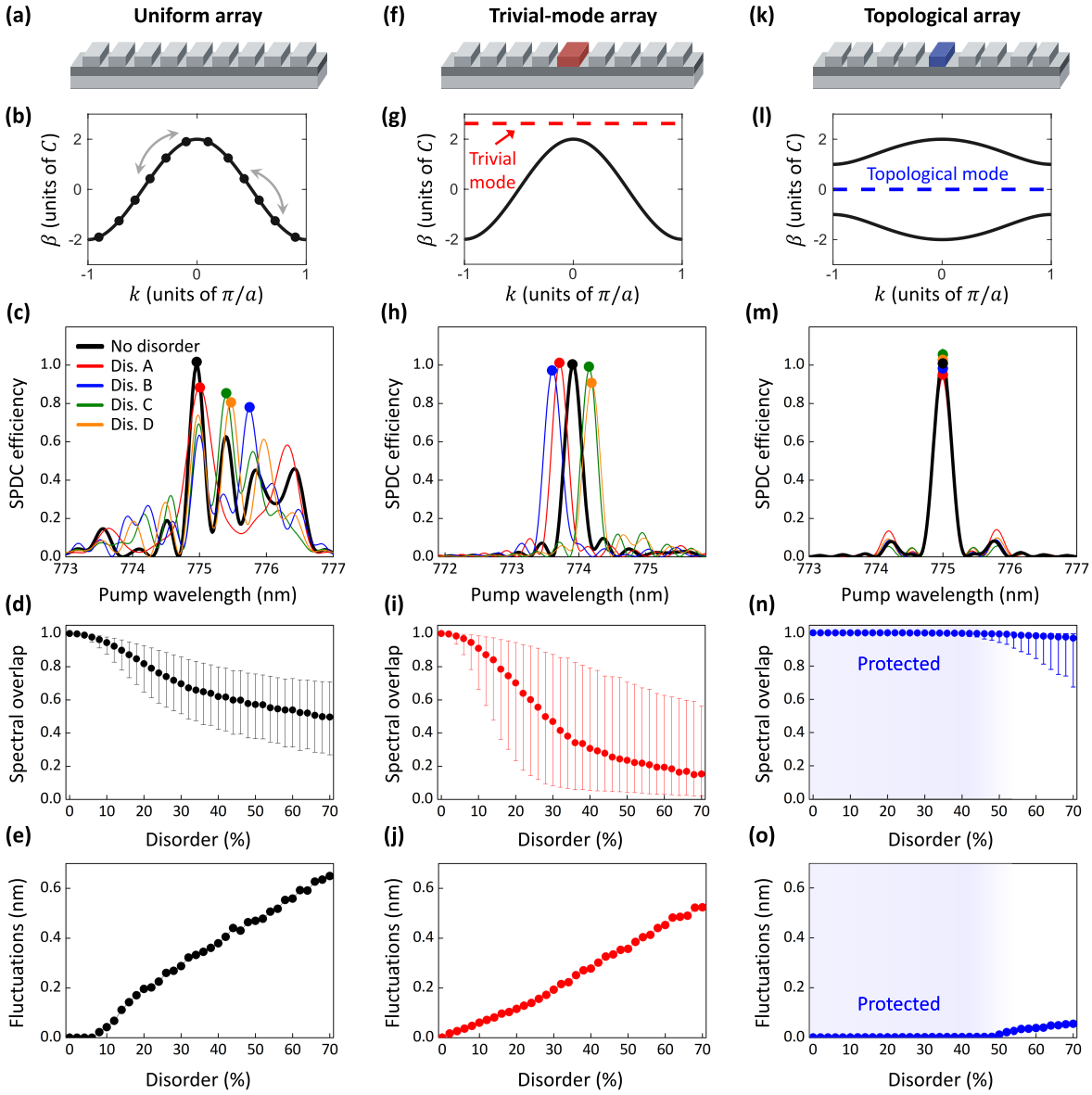


FIG. 2. First column: (a) schematic transverse view and (b) band structure of a uniform waveguide array. (c) Calculated SPDC resonance spectra in the absence of disorder (bold black line) and for 4 different disorder realizations (thin colored lines) with disorder strength $\Delta = 40\%$ in the coupling constants, with pump injection and photon-pair collection in the central waveguide. The SPDC efficiency is shown in arbitrary units. (d) Median and spread (16th–84th percentiles) of the overlap between each disordered resonance spectrum and the disorder-free spectrum, calculated over 1000 realizations as a function of disorder strength. (e) Standard deviation of the resonance-peak wavelength as a function of disorder strength. Second column, panels (f)–(j): same quantities for an array featuring a trivial localized mode at its center, resulting from a larger central waveguide [red in panel (f)]. Third column, panels (k)–(o): same quantities for a topological array implementing the Su-Schrieffer-Heeger model, with alternating coupling constants $C(1+K)$ and $C(1-K)$, dimerization parameter $K = 0.5$, and a topological interface at the center (blue). Simulation parameters: all arrays contain 13 waveguides of length $L = 2$ mm, with coupling constant $C = 4$ mm^{-1} and pump coupling parameter $\alpha = 0.1$; the modal dispersions correspond to the AlGaAs waveguides considered in the experiments (see text). In panels (b,g,l), the schematic band structures show the propagation constant β relative to that of an isolated waveguide versus the Bloch wave vector k (in units of π/a, with a the lattice period). The bulk bands (bold lines) correspond to infinite periodic lattices. Black dots in (b) schematically illustrate the bulk eigenmodes of a finite uniform array, while dashed lines in (g) and (l) mark the propagation constants of localized modes.

creates a signal (idler) photon in supermode m_s (m_i), A_{m_p} is the pump amplitude in supermode m_p, and γ_j denotes the nonlinear overlap integral of the three interacting modes for the combination j. The corresponding phase mismatch reads

$$\Delta\beta_j(\omega_p) = \beta^p_{m_p} - \beta^s_{m_s} - \beta^i_{m_i}. \tag{3}$$

In a uniform array, all supermodes are *bulk modes* (modes delocalized across the array and belonging to the propagation band) in the absence of disorder. Pumping the central waveguide excites multiple pump supermodes, which can then down-convert into several combinations of signal and idler bulk modes, as schematically illustrated by gray arrows in Fig. 2(b). Disorder alters both the propagation constants and spatial profiles of these modes, thereby modifying the phase-matching frequencies and overlap integrals, respectively. This naturally leads to strong fluctuations in both the shape and peak position of the resonance spectrum, consistent with the numerical findings of Fig. 2 (first column).

In contrast, both SSH and trivial-mode arrays support a localized supermode that is efficiently excited by central pumping. The dominant SPDC interaction then involves localized pump, signal, and idler modes, yielding a narrow, single-peak spectrum characteristic of a single-mode process. The crucial difference lies in the behavior of the propagation constant of this mode: in the SSH array it is protected by the underlying chiral symmetry (both for the pump and the SPDC fields), whereas no such protection exists in the trivial configuration. As a result, the phase-matching condition associated with this mode remains stable in the SSH array, while it fluctuates with disorder in the trivial case. Consequently, only the topological array preserves both the shape and the central wavelength of its resonance spectrum, up to significant disorder levels. Beyond this protection against coupling disorder, the SSH array also provides enhanced resilience to waveguide-width fluctuations compared with an isolated waveguide, as will be discussed below [Fig. 5(f)].

The supermode model of Eq. (2) also explains the onset of small disorder-induced fluctuations once the disorder strength becomes comparable to the dimerization parameter K (here 50%), as seen in Figs. 2(n) and 2(o). At this point, disorder can locally invert the alternation between short and long couplings and significantly modify the modal structure: the original topological supermode may shift spatially or broaden, while some bulk modes may localize near the central (pumped) waveguide and approach the propagation constant of the topological mode. As a result, additional channels involving pump and/or down-converted photons in disorder-sensitive bulk modes progressively gain importance [33]. Their relative weight is governed by the nonlinear overlap integrals γ_j and phase-matching sinc factors appearing in Eq. (2), both of which evolve as disorder modifies the modal structure. This produces a crossover from a protected to a more disorder-sensitive nonlinear response beyond $\Delta \approx K$. The resulting fluctuations nevertheless remain much smaller than in non-topological arrays, because the topological channel still dominates the SPDC interaction and thereby ensures effective stabilization of the resonance against coupling disorder.

III. EXPERIMENTS

We now turn to the experimental verification of these predictions. The three lattice geometries investigated above were fabricated using AlGaAs, which combines a strong $\chi^{(2)}$ nonlinearity and mature nanofabrication technology [47]. Each array consists of 13 waveguides with a length of $L = 2$ mm and a width of 2 μm. The arrays were patterned by electron-beam lithography with a high-resolution HSQ resist, followed by inductively coupled plasma (ICP) etching. As sketched in Fig. 1, the epitaxial structure comprises a 6-period $Al_{0.8}Ga_{0.2}As/Al_{0.25}Ga_{0.75}As$ lower Bragg reflector, a 350 nm $Al_{0.45}Ga_{0.55}As$ core, and a 4-period $Al_{0.8}Ga_{0.2}As/Al_{0.25}Ga_{0.75}As$ upper Bragg reflector. The two Bragg mirrors provide vertical photonic band-gap confinement for the pump beam in the near-infrared, while ensuring total internal reflection for the down-converted photons in the telecom range. As a result, the pump and SPDC modes exhibit distinct dispersion relations, enabling the single-waveguide phase-matching condition to be satisfied within the spectral range of interest [14,15,48–50]. The central waveguide comprises enlarged input and output sections (6 μm wide) connected to the array through tapers, as shown in the SEM image in Fig. 3. These enlarged sections shift the local nonlinear resonance wavelength, ensuring that photon pairs are generated exclusively within the central array region.

For the uniform arrays, the inter-waveguide distance, defined edge-to-edge, is 1100 nm, and the etching depth reaches the first layer above the core, yielding a mean simulated coupling constant $C = 4$ mm^{-1} (3.5 mm^{-1} for TE and 4.5 mm^{-1} for TM polarization) for the SPDC photons and a pump coupling parameter $\alpha = C_p/C \simeq 0.1$, in good agreement with direct measurements based on laser-beam propagation [40]. For the topological SSH array, a dimerization $K = 0.5$, centered around the same mean coupling as in the uniform array, is obtained by alternating 870 and 1700 nm inter-waveguide distances, as shown in the close-up SEM image of Fig. 3. Finally, for the trivial-mode array, the central waveguide width is 2.1 μm and the inter-waveguide distance is 1000 nm, yielding a defect amplitude identical to that used in the simulations and chosen to reproduce a localization length similar to that of the SSH array. Typical propagation losses of the fabricated structures are about 1 cm^{-1} at telecom wavelengths.

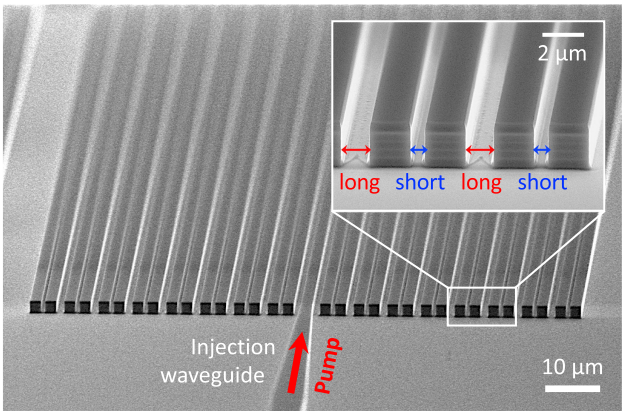


FIG. 3. SEM image of an AlGaAs topological SSH array (here comprising 31 waveguides) with an injection waveguide for the pump beam. The inset shows a close-up of the alternating short (870 nm) and long (1700 nm) spacings between adjacent waveguides, resulting in alternating high and low coupling constants.

To investigate the effect of disorder, we intentionally varied the inter-waveguide distances around their nominal values and fabricated a series of samples corresponding to different random disorder realizations spanning a representative statistical ensemble. The experiments are then performed by injecting a tunable TE-polarized continuous-wave pump laser into the central waveguide of each array using a microscope objective, with a coupled power of 1 mW. Orthogonally polarized signal and idler photons are generated via type-II SPDC and collected from the central waveguide with a second microscope objective. The SPDC photons are then coupled into an optical fiber, split by a fiber polarizing beamsplitter, and detected by superconducting nanowire single-photon detectors after passing through a high-pass filter with a cutoff wavelength of 1500 nm. The filter transmission, together with energy conservation, defines an effective detection bandwidth of $\simeq$100 nm for the SPDC photons.

Resonance spectra are obtained by tuning the wavelength of the pump laser (Toptica DL pro) in 60 pm steps using a motorized scanning routine, while monitoring the coincidence counts collected from the central waveguide. Figure 4(a) shows the SPDC resonance spectra, defined as the signal-idler raw coincidence counts measured as a function of pump wavelength, in a uniform waveguide array without disorder (bottom trace) and for several disorder realizations with amplitude $\Delta = 40\%$. All spectra are normalized to unity and vertically offset for clarity. The pump-wavelength window shown in Figs. 4(a)–4(c) was chosen to focus on the main resonance region (it does not represent a spectral boundary of the SPDC emission). Strong fluctuations are observed in both the spectral shape and the resonance-peak position (marked by black dots). The standard deviation of the peak position is 0.79 nm, and the median overlap between the spectra is 0.37. We checked that the raw spectra exhibit comparable peak coincidence counts ($\sim$200) across disorder realizations and lattice geometries, indicating sufficient signal levels and comparable Poissonian counting uncertainties. We further verified that either subtracting the measured accidental background or normalizing the coincidence counts by it does not change the extracted resonance-peak positions within the measurement resolution, confirming the consistency of their experimental determination.

We next investigate arrays supporting a trivial localized mode at the center. The corresponding SPDC resonance spectra, shown in Fig. 4(b), exhibit a generally more regular shape, but the resonance-peak positions still display large fluctuations. Here, the standard deviation of the peak position is 0.65 nm, and the median spectral overlap is 0.30.

Finally, Fig. 4(c) presents resonance spectra measured in the topological SSH arrays. In this case, a much-improved stability is observed, both in the general spectral shape and in the resonance-peak position. The standard deviation of the peak position is reduced to 0.075 nm (which approaches the 0.06 nm resolution of the pump laser tuning), while the median overlap increases to 0.81. At the resonance peak, the generation rate in the SSH arrays is on the order of 10^5 pairs.s^{-1}.

The experimental results for the three types of arrays are summarized in Fig. 4(d) (resonance-peak fluctuations) and Fig. 4(e) (spectral overlap) with blue vertical bars. To investigate the scaling of spectral fluctuations with the disorder strength, we repeated the same measurements on a second series of samples with a reduced disorder amplitude of 20%. The corresponding results are shown in Figs. 4(d) and 4(e) with red vertical bars. In good qualitative agreement with the simulations of Fig. 2, reducing the disorder amplitude from 40% to 20% leads, in all three cases, to a decrease in resonance-peak fluctuations together with an increase in spectral overlap. For the topological arrays, the resonance fluctuations are reduced to about 0.02 nm, while they are respectively 12 and 27 times larger in the trivial-mode and uniform arrays. In addition, the spectral overlap rises to 0.9 in the SSH arrays, highlighting the strongly reduced influence of disorder on the entire resonance spectrum. At 40% disorder, the slight residual resonance-peak fluctuations (0.075 nm) likely arise from the proximity to the point where resonance stabilization begins to weaken ($\Delta \approx K$), as shown in Figs. 2(n) and 2(o). A slightly lower effective dimerization parameter K in the fabricated structure may therefore already place the system at the onset of this regime.

We thus find good qualitative agreement with the simulations of Fig. 2, based on Eq. (1), which assumes identical polarization and perfect spectral degeneracy of the SPDC photons and captures the essential physics within a minimal framework. A more quantitative

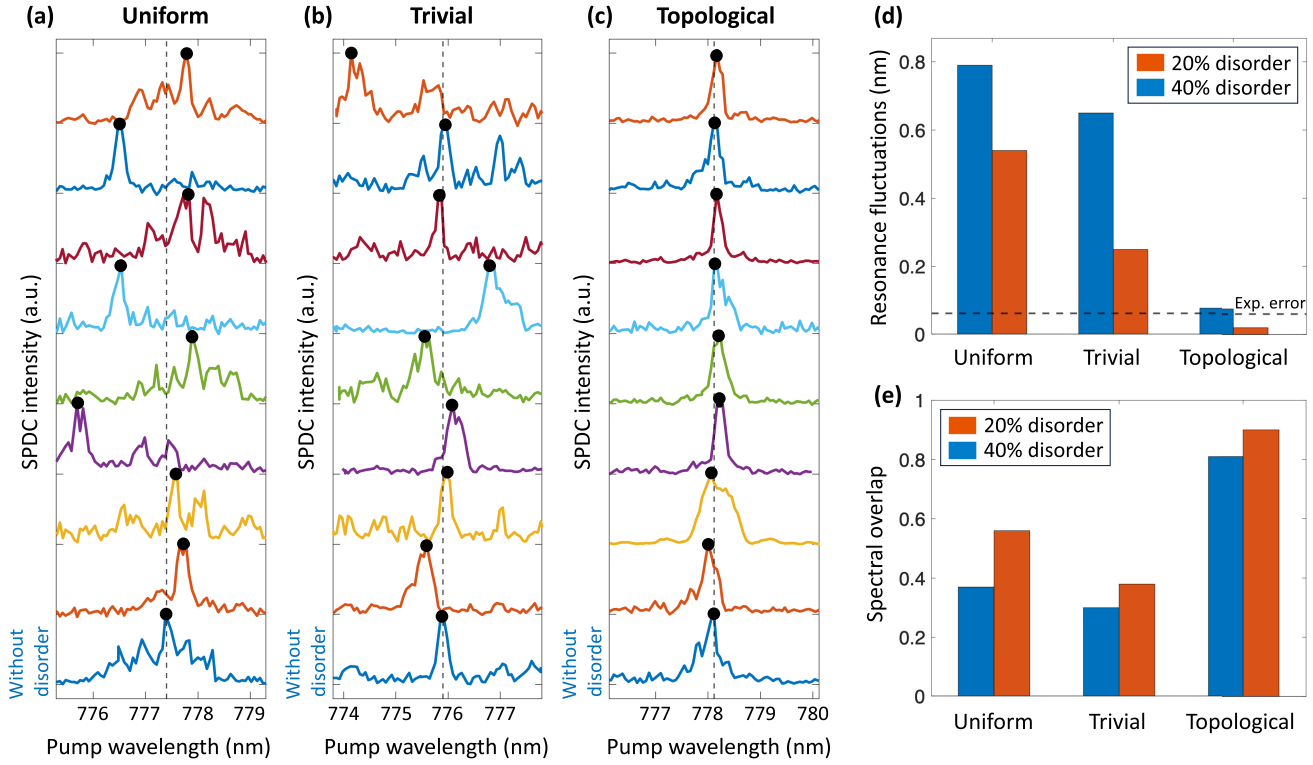


FIG. 4. (a) Measured SPDC resonance spectra in uniform waveguide arrays without disorder (bottom trace) and for various random disorder realizations with amplitude $\Delta = 40\%$. (b) Same measurement for arrays featuring a trivial localized mode at the center, and (c) for topological SSH arrays. All spectra are normalized to unity and vertically offset for clarity. (d) Experimental fluctuations (standard deviation) of the resonance-peak wavelength for the three types of arrays at coupling disorder strengths $\Delta = 40\%$ (blue bars) and $\Delta = 20\%$ (red bars). (e) Median pairwise overlap between the SPDC resonance spectra, under the same conditions as in (d).

description can be obtained by extending this formalism to account for type-II polarizations, the finite spectral bandwidth of the photons, and the associated polarization and frequency dependence of the coupling constants (see Supplemental Material [40]). This extended analysis confirms that the stabilization of the SSH resonance spectrum persists beyond the idealized degenerate model, remaining effective when polarization and spectral non-degeneracies are included and across all detection bandwidths considered. By contrast, the simplified model (Fig. 2) shows that non-topological arrays already exhibit significant resonance fluctuations in the *a priori* most favorable limit of co-polarized photons degenerate in frequency. Overall, these results establish that the topological stabilization of the resonance is robust to the detailed dynamics of the parametric process. Numerical simulations further indicate that this protection is not specific to the local coincidence observable chosen for our experiment. It extends to first-order intensity observables, including the total single-count signal, showing that the resonance stabilization extends to both local and global observables [40].

IV. DISCUSSION AND PERSPECTIVES

Having experimentally demonstrated the robustness of the SPDC resonance spectrum of SSH arrays to coupling disorder, an important question is whether this robustness also extends to the biphoton emission spectrum [34]. Indeed, ensuring that independent parametric sources emit quantum states with identical spectra is essential for achieving high-visibility quantum interference [35,37,51]. Such interference underpins many quantum information tasks, from quantum computing and simulation to the generation of high-dimensional entangled states [1,52].

We investigate how disorder affects the biphoton spectrum in the different arrays considered above through numerical simulations. Figure 5(a) shows the calculated joint spectral intensity ($|\phi(\omega)|^2$) of photon pairs emitted from the central waveguide of a uniform array (using the same parameters as in Fig. 2), in the absence of disorder (bold black line) and for various random disorder realizations (thin colored lines) with $\Delta = 40\%$. Owing to strict energy conservation under cw pumping, the joint spectral amplitude ϕ depends on a single frequency variable ω, such that $\phi(\omega_s, \omega_i) = \phi(\omega_s, \omega_p - \omega_s) \equiv \phi(\omega)$. The pump wavelength is tuned to the maximum of the resonance spectrum of the disorder-free array. Similarly, Figs. 5(b) and 5(c) show the joint spectra calculated in trivial-mode arrays and SSH arrays, respectively. While large spectral fluctuations are observed for uniform and trivial-mode arrays, the biphoton spectra of the topological arrays remain remarkably stable under disorder.

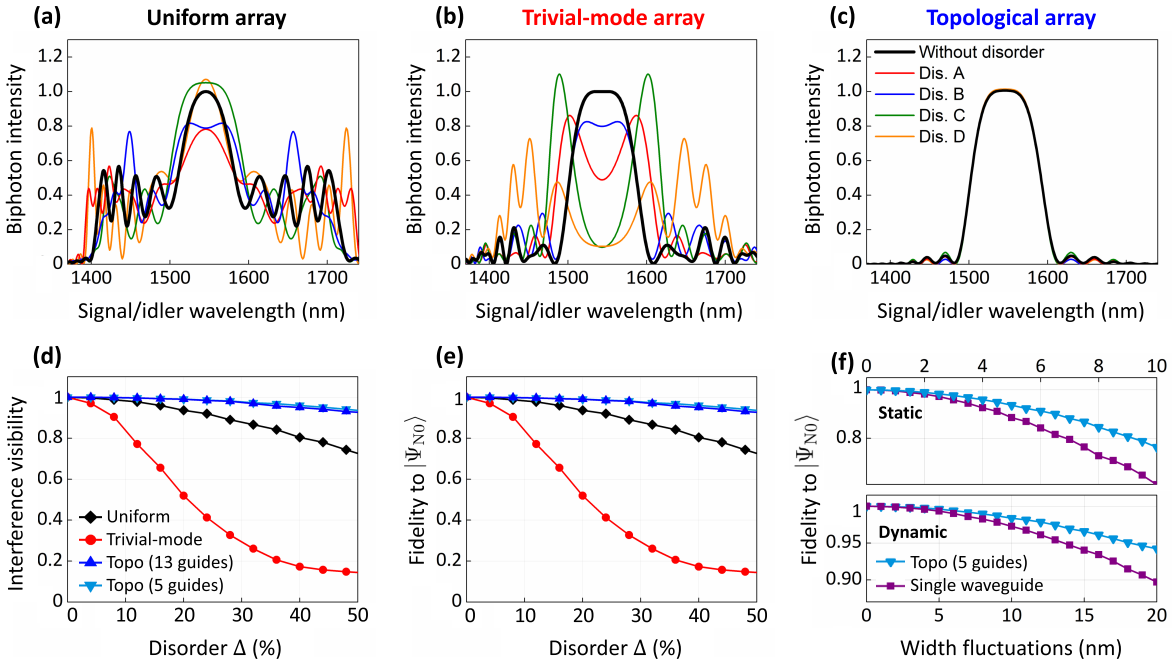


FIG. 5. (a) Joint spectral intensity $|\phi(\omega)|^2$ of photon pairs emitted from the central waveguide of a uniform waveguide array, calculated in the absence of disorder (bold black line) and for 4 different disorder realizations (thin colored lines) with disorder strength $\Delta = 40\%$ in the coupling constants. The pump wavelength is tuned to the maximum of the resonance spectrum in the absence of disorder. (b) Joint spectral intensity calculated for trivial-mode arrays and (c) topological SSH arrays. The vertical scale in panels (a)–(c) is in arbitrary units. (d) Mean interference visibility $\bar{V} = \langle V_{n,n'} \rangle$ between pairs of sources [Eq. (4)], calculated as a function of coupling disorder, for uniform (black), trivial-mode (red) and topological SSH arrays with 13 waveguides (blue) or 5 waveguides (light blue). (e) Mean fidelity $\bar{\mathcal{F}}$ to an ideal broadband (100 nm) maximally path-entangled state prepared by coherently pumping 10 biphoton sources, calculated as a function of coupling disorder (same color code). (f) Mean fidelity [as in (e)] versus waveguide-width fluctuations, for 5-waveguide SSH arrays (light blue) and single-waveguide sources (purple). Top: static disorder. Bottom: longitudinally varying disorder (see text).

Here, each array is pumped and collected through its central waveguide, and therefore behaves as an effective photon-pair source emitting into a single spatial mode (while its emission spectrum remains shaped by the full lattice modal structure). This raises the question of how stable the interference between such effective sources remains in the presence of disorder. To address this question, we first consider two independent effective sources pumped by the same continuous-wave laser. Their outputs interfere on a balanced beamsplitter, forming the time-reversed analog of the Hong-Ou-Mandel experiment [9,35,37,53–56]. Perfect antibunching occurs when the two sources emit biphotons with identical spectra and equal generation efficiencies, while spectral or efficiency mismatches reduce the interference visibility. For two sources n and n', the visibility can be written as [40]

$$V_{n,n'} = 2\sqrt{P_n P_{n'}}\,\mathrm{Re}\left[\int d\omega\, \phi_n^*(\omega)\phi_{n'}(\omega)\right], \qquad (4)$$

where P_n and $P_{n'}$ denote the probabilities for generating the photon pair in sources n and n' (under identical pump power), with $P_n + P_{n'} = 1$, $\phi_n(\omega)$ and $\phi_{n'}(\omega)$ are the normalized joint spectral amplitudes, and Re denotes the real part. The interference visibility therefore provides a comprehensive figure of merit, capturing both resonance stability (via the generation probabilities) and the joint spectral amplitude of the generated photons.

We compute the biphoton states for many realizations of coupling disorder (1000), each corresponding to a distinct source, and evaluate the mean visibility $\bar{V} = \langle V_{n,n'} \rangle$ over all pairs of sources. Figure 5(d) shows the evolution of $\bar{V}$ as a function of the disorder strength. For the topological SSH array (blue), a high interference visibility is preserved, remaining above 95% up to 40% disorder. For comparison, results for uniform and trivial-mode arrays are also shown (black and red), and degrade more rapidly as disorder increases. This behavior, which is particularly pronounced for the trivial-mode array, further demonstrates that mere spatial localization of the SPDC modes is not sufficient to ensure robustness against disorder, highlighting the protective role of the SSH configuration. The same figure also shows results obtained for an SSH array comprising only 5 waveguides (light blue). Interestingly, the performance is very similar to that of the 13-waveguide SSH array, showing that surrounding the central waveguide

with just two neighbors on each side, forming a minimal SSH unit, is already sufficient to achieve efficient protection, while minimizing the footprint on the chip.

Beyond pairwise interference, large-scale quantum photonic circuits require many independent sources to emit mutually indistinguishable quantum states. We therefore examine a more demanding scenario in which N parametric sources are pumped simultaneously by the same laser. In the ideal case, all sources emit identical biphoton spectra $\phi_n(\omega) \equiv \phi_0(\omega)$ and have equal generation efficiencies, such that the resulting state is $|\Psi_{N0}\rangle = \frac{1}{\sqrt{N}}\sum_{n=1}^{N} |\phi_0\rangle_n$. It constitutes a broadband, maximally path-entangled state, namely a coherent superposition of indistinguishable biphotons across N different spatial modes. To quantify deviations from this ideal situation, we evaluate the fidelity $\mathcal{F}$ between the generated state and the ideal one [40]. Figure 5(e) shows, for path-entangled states constructed with $N = 10$ sources over a 100 nm spectral bandwidth, the mean fidelity $\bar{\mathcal{F}}$ as a function of the disorder strength. A trend similar to that observed for the two-source interference visibility is found. The topological SSH array (with 13 or 5 waveguides) outperforms the non-topological arrays, with a mean fidelity to the ideal state $|\Psi_{N0}\rangle$ above 96% up to 40% coupling disorder.

Finally, we examine the impact of waveguide width fluctuations, which modify the propagation constants β of the SPDC and pump modes. In the SSH model, such perturbations break chiral symmetry and therefore lift exact topological protection [45,57]. We here benchmark topological arrays against conventional single-waveguide sources, which provide a natural reference system for such disorder. For a conservative comparison, we assume that width fluctuations in the topological arrays also affect the corresponding inter-waveguide distances, thereby inducing disorder in the coupling constants as well. Figure 5(f) compares the mean fidelity $\bar{\mathcal{F}}$ to the maximally path-entangled state $|\Psi_{N0}\rangle$ as a function of width fluctuations, for SSH arrays comprising five waveguides (light blue) and for single waveguides (purple). The upper panel corresponds to static width inhomogeneities (constant along z), while the lower panel considers longitudinally varying fluctuations (with a correlation length of 100 μm, representative, for example, of stitching-field errors in the electron-beam lithography process). Interestingly, SSH arrays consistently outperform single-waveguide sources, for both static and dynamic disorder. This enhanced robustness arises from the reduced sensitivity of the supermode propagation constant to local width fluctuations. Indeed, in a single waveguide, phase matching directly depends on the local propagation constant and is therefore fully exposed to disorder, whereas the collective nature of the topological SSH supermode averages over individual waveguide perturbations, thereby mitigating their impact. This mechanism relies on inter-waveguide coupling, which could in principle introduce an additional sensitivity to disorder that is absent in a single waveguide. However, the SSH configuration is precisely resilient to these perturbations: the off-diagonal disorder associated with inter-waveguide distance fluctuations was included in the simulations of Fig. 5(f) for completeness, but we verified that it does not affect the fidelity (within numerical precision). The topological system can therefore exploit the self-averaging of diagonal perturbations provided by the collective supermode while remaining protected against coupling disorder, making it a well-suited platform for photon-pair generation with enhanced robustness against various types of fabrication imperfections.

In conclusion, by systematically comparing uniform, trivial-mode, and topological SSH nonlinear waveguide arrays, we have experimentally established the topological robustness of the SPDC resonance spectrum in SSH arrays and identified its origin in the stability of the underlying interacting modes. To our knowledge, this provides the first experimental evidence of such protection in a one-dimensional photonic system, opening the way for simple and compact on-chip implementations. Numerical analysis further predicts that this robustness extends to the spectral properties of the emitted biphoton states, highlighting the potential of topological waveguide arrays to realize robust photon-pair sources enabling high-visibility quantum interference and the generation of broadband high-dimensional entangled states with high fidelity.

The present analysis also clarifies the conditions under which these topological advantages become experimentally observable, and provides a concrete basis for their implementation in suitably designed devices supporting multi-source operation and readout. As we have shown, efficient protection already arises in small SSH units with as few as five waveguides. Compact architectures could therefore be envisioned, in which several topological interfaces [as sketched in blue in Fig. 2(k)] are periodically embedded along a single chain [58]. For sufficiently large dimerization, the interface states have negligible mutual overlap while each remains embedded in a local SSH environment, allowing the corresponding interfaces to operate as independent and robust photon-pair sources and thereby forming a compact multi-source architecture. Beyond this specific implementation, our approach could be extended to emerging material platforms that do not yet benefit from mature fabrication [1,59], thereby mitigating imperfections and leveraging topology as a practical route toward resilient quantum photonic circuits.

Looking further ahead, the versatility of the present platform also paves the way for extending topological effects into synthetic dimensions, where internal degrees of freedom, such as frequency modes, emulate additional propagation directions [60]. Indeed, the strong electro-optic response of AlGaAs [47,61] in a traveling-wave geometry could provide controlled motion along a

synthetic frequency axis in addition to the spatial dimension [62,63]. This would open the way to protected frequency conversion or hybrid entanglement across time, space, and frequency degrees of freedom [62], enabling quantum information processing across multiple dimensions. Nonlinear waveguide arrays thus offer a versatile platform to explore topological effects in the quantum regime and design novel, topology-driven optical functionalities.

ACKNOWLEDGMENTS

We thank A. Raymond, L. Lazzari, F. Raineri, E. Descamps and P. Milman for fruitful discussions and P. Filloux, B. Janvier and M. Nicolas for technical support. We acknowledge support from the Ville de Paris Emergence program (LATTICE project), Région Île-de-France in the framework of the DIM QuanTiP (Q-LAT project), IdEx Université Paris Cité (ANR-18-IDEX-0001), the Plan France 2030 through the PEPR NISQ2LSQ project (ANR-22-PETQ-0006), the French National Research Agency (ANR) through the EQUIPPS project (ANR-24-CE97-0003), and the "Investissement d'Avenir" program of the French Government through the QuanTEdu-France project (ANR-22-CMAS-0001). We acknowledge the use of cleanroom facilities from the "Groupement des Plateformes de Micro et Nanotechnologies de Paris" and support from Université Paris Cité, CNRS, RENATECH+ and RENATECH project (ANR-22-PEEL-0015) from PEPR Electronique for micro- and nanofabrication.

DATA AVAILABILITY

The data that support the findings of this article are not publicly available upon publication because it is not technically feasible and/or the cost of preparing, depositing, and hosting the data would be prohibitive within the terms of this research project. The data are available from the authors upon reasonable request.

[1] J. Wang, F. Sciarrino, A. Laing, and M. G. Thompson, *Integrated photonic quantum technologies*, Nat. Photonics **14**, 273 (2020).

[2] Y. Bromberg, Y. Lahini, R. Morandotti, and Y. Silberberg, *Quantum and classical correlations in waveguide lattices*, Phys. Rev. Lett. **102**, 253904 (2009).

[3] A. Peruzzo, M. Lobino, J. C. Matthews, N. Matsuda, A. Politi, K. Poulios, X.-Q. Zhou, Y. Lahini, N. Ismail, K. Wörhoff *et al.*, *Quantum walks of correlated photons*, Science **329**, 1500 (2010).

[4] A. S. Solntsev, F. Setzpfandt, A. S. Clark, C. W. Wu, M. J. Collins, C. Xiong, A. Schreiber, F. Katzschmann, F. Eilenberger, R. Schiek, W. Sohler, A. Mitchell, C. Silberhorn, B. J. Eggleton, T. Pertsch, A. A. Sukhorukov, D. N. Neshev, and Y. S. Kivshar, *Generation of nonclassical biphoton states through cascaded quantum walks on a nonlinear chip*, Phys. Rev. X **4**, 031007 (2014).

[5] R. J. Chapman, M. Santandrea, Z. Huang, G. Corrielli, A. Crespi, M.-H. Yung, R. Osellame, and A. Peruzzo, *Experimental perfect state transfer of an entangled photonic qubit*, Nat. Commun. **7**, 11339 (2016).

[6] M. C. Rechtsman, Y. Lumer, Y. Plotnik, A. Perez-Leija, A. Szameit, and M. Segev, *Topological protection of photonic path entanglement*, Optica **3**, 925 (2016).

[7] M. Gräfe, R. Heilmann, M. Lebugle, D. Guzman-Silva, A. Perez-Leija, and A. Szameit, *Integrated photonic quantum walks*, J. Opt. **18**, 103002 (2016).

[8] J.-L. Tambasco, G. Corrielli, R. J. Chapman, A. Crespi, O. Zilberberg, R. Osellame, and A. Peruzzo, *Quantum interference of topological states of light*, Sci. Adv. **4**, eaat3187 (2018).

[9] A. Blanco-Redondo, B. Bell, D. Oren, B. J. Eggleton, and M. Segev, *Topological protection of biphoton states*, Science **362**, 568 (2018).

[10] Y. Lahini, G. R. Steinbrecher, A. D. Bookatz, and D. Englund, *Quantum logic using correlated one-dimensional quantum walks*, npj Quantum Inf. **4**, 2 (2018).

[11] D. Barral, M. Walschaers, K. Bencheikh, V. Parigi, J. A. Levenson, N. Treps, and N. Belabas, *Quantum state engineering in arrays of nonlinear waveguides*, Phys. Rev. A **102**, 043706 (2020).

[12] D. Barral, K. Bencheikh, J. A. Levenson, and N. Belabas, *Scalable multimode entanglement based on efficient squeezing of propagation eigenmodes*, Phys. Rev. Res. **3**, 013068 (2021).

[13] F. Hoch, S. Piacentini, T. Giordani, Z.-N. Tian, M. Iuliano, C. Esposito, A. Camillini, G. Carvacho, F. Ceccarelli, N. Spagnolo *et al.*, *Reconfigurable continuously-coupled 3D photonic circuit for boson sampling experiments*, npj Quantum Inf. **8**, 55 (2022).

[14] A. Raymond, A. Zecchetto, J. Palomo, M. Morassi, A. Lemaître, F. Raineri, M. I. Amanti, S. Ducci, and F. Baboux, *Tunable generation of spatial entanglement in nonlinear waveguide arrays*, Phys. Rev. Lett. **133**, 233602 (2024).

[15] A. Raymond *et al.*, *Tailoring quantum walks in integrated photonic lattices*, Opt. Express **33**, 45869 (2025).

[16] R. J. Chapman, S. Häusler, G. Finco, F. Kaufmann, and R. Grange, *Quantum logical controlled-NOT gate in a lithium niobate-on-insulator photonic quantum walk*, Quantum Sci. Technol. **9**, 015016 (2023).

[17] Y. Yang, R. J. Chapman, A. Youssry, B. Haylock, F. Lenzini, M. Lobino, and A. Peruzzo, *Programmable quantum circuits in a large-scale photonic waveguide array*, npj Quantum Inf. **11**, 19 (2025).

[18] H. B. Perets, Y. Lahini, F. Pozzi, M. Sorel, R. Morandotti, and Y. Silberberg, *Realization of quantum walks with negligible decoherence in waveguide lattices*, Phys. Rev. Lett. **100**, 170506 (2008).

[19] G. Di Giuseppe, L. Martin, A. Perez-Leija, R. Keil, F. Dreisow, S. Nolte, A. Szameit, A. F. Abouraddy, D. N. Christodoulides, and B. E. A. Saleh, *Einstein-Podolsky-Rosen spatial entanglement in ordered and Anderson photonic lattices*, Phys. Rev. Lett. **110**, 150503 (2013).

[20] M. Lebugle, M. Gräfe, R. Heilmann, A. Perez-Leija, S. Nolte, and A. Szameit, *Experimental observation of N00N state Bloch oscillations*, Nat. Commun. **6**, 8273 (2015).
[21] F. Caruso, A. Crespi, A. G. Ciriolo, F. Sciarrino, and R. Osellame, *Fast escape of a quantum walker from an integrated photonic maze*, Nat. Commun. **7**, 11682 (2016).
[22] D. N. Biggerstaff, R. Heilmann, A. A. Zecevik, M. Gräfe, M. A. Broome, A. Fedrizzi, S. Nolte, A. Szameit, A. G. White, and I. Kassal, *Enhancing coherent transport in a photonic network using controllable decoherence*, Nat. Commun. **7**, 11282 (2016).
[23] T. Ozawa, H. M. Price, A. Amo, N. Goldman, M. Hafezi, L. Lu, M. C. Rechtsman, D. Schuster, J. Simon, O. Zilberberg *et al.*, *Topological photonics*, Rev. Mod. Phys. **91**, 015006 (2019).
[24] J. Gao, Z.-S. Xu, Z. Yang, V. Zwiller, and A. W. Elshaari, *Quantum topological photonics with special focus on waveguide systems*, npj Nanophotonics **1**, 34 (2024).
[25] A. Hashemi, M. J. Zakeri, P. S. Jung, and A. Blanco-Redondo, *Topological quantum photonics*, APL Photonics **10**, 010903 (2025).
[26] Y. Wang, X.-L. Pang, Y.-H. Lu, J. Gao, Y.-J. Chang, L.-F. Qiao, Z.-Q. Jiao, H. Tang, and X.-M. Jin, *Topological protection of two-photon quantum correlation on a photonic chip*, Optica **6**, 955 (2019).
[27] Y. Wang, Y.-H. Lu, J. Gao, Y.-J. Chang, R.-J. Ren, Z.-Q. Jiao, Z.-Y. Zhang, and X.-M. Jin, *Topologically protected polarization quantum entanglement on a photonic chip*, Chip **1**, 100003 (2022).
[28] D. Leykam, A. S. Solntsev, A. A. Sukhorukov, and A. S. Desyatnikov, *Lattice topology and spontaneous parametric down-conversion in quadratic nonlinear waveguide arrays*, Phys. Rev. A **92**, 033815 (2015).
[29] Y. Yang, Z. Zuo, and D. Cao, *Biphoton topology in a quadratic nonlinear waveguide array under the Su-Schrieffer-Heeger model*, Phys. Rev. A **104**, 043710 (2021).
[30] D. Wang, Q. Qiu, Y. Zhao, X. Jing, X. Zheng, S. Zhao, Y. Tao, G. Liu, C. Sheng, and L. Lu, *Topological localization of biphoton states in arrays of nonlinear photonic waveguides*, Phys. Rev. A **113**, 023502 (2026).
[31] R.-J. Ren, Y.-H. Lu, Z.-K. Jiang, J. Gao, W.-H. Zhou, Y. Wang, Z.-Q. Jiao, X.-W. Wang, A. S. Solntsev, and X.-M. Jin, *Topologically protecting squeezed light on a photonic chip*, Photonics Res. **10**, 456 (2022).
[32] M. Wang, C. Doyle, B. Bell, M. J. Collins, E. Magi, B. J. Eggleton, M. Segev, and A. Blanco-Redondo, *Topologically protected entangled photonic states*, Nanophotonics **8**, 1327 (2019).
[33] N. Bergamasco and M. Liscidini, *Generation of photon pairs in topologically protected guided modes*, Phys. Rev. A **100**, 053827 (2019).
[34] S. Mittal, E. A. Goldschmidt, and M. Hafezi, *A topological source of quantum light*, Nature (London) **561**, 502 (2018).
[35] J. W. Silverstone, D. Bonneau, K. Ohira, N. Suzuki, H. Yoshida, N. Iizuka, M. Ezaki, C. M. Natarajan, M. G. Tanner, R. H. Hadfield *et al.*, *On-chip quantum interference between silicon photon-pair sources*, Nat. Photonics **8**, 104 (2014).
[36] J. Wang, S. Paesani, Y. Ding, R. Santagati, P. Skrzypczyk, A. Salavrakos, J. Tura, R. Augusiak, L. Mančinska, D. Bacco *et al.*, *Multidimensional quantum entanglement with large-scale integrated optics*, Science **360**, 285 (2018).
[37] R. J. Chapman, T. Kuttner, J. Kellner, A. Sabatti, A. Maeder, G. Finco, F. Kaufmann, and R. Grange, *On-chip quantum interference between independent lithium niobate-on-insulator photon-pair sources*, Phys. Rev. Lett. **134**, 223602 (2025).
[38] A. S. Solntsev, A. A. Sukhorukov, D. N. Neshev, and Y. S. Kivshar, *Spontaneous parametric down-conversion and quantum walks in arrays of quadratic nonlinear waveguides*, Phys. Rev. Lett. **108**, 023601 (2012).
[39] M. Gräfe, A. Solntsev, R. Keil, A. Sukhorukov, M. Heinrich, A. Tünnermann, S. Nolte, A. Szameit, and Y. S. Kivshar, *Biphoton generation in quadratic waveguide arrays: A classical optical simulation*, Sci. Rep. **2**, 562 (2012).
[40] See Supplemental Material at http://link.aps.org/supplemental/10.1103/kszt-p63d for additional details on the experiment, theoretical framework, and numerical simulations, which includes Refs. [41,42].
[41] R. T. Horn, P. Kolenderski, D. Kang, P. Abolghasem, C. Scarcella, A. Della Frera, A. Tosi, L. G. Helt, S. V. Zhukovsky, J. E. Sipe *et al.*, *Inherent polarization entanglement generated from a monolithic semiconductor chip*, Sci. Rep. **3**, 2314 (2013).
[42] R. Kruse, F. Katzschmann, A. Christ, A. Schreiber, S. Wilhelm, K. Laiho, A. Gábris, C. S. Hamilton, I. Jex, and C. Silberhorn, *Spatio-spectral characteristics of parametric down-conversion in waveguide arrays*, New J. Phys. **15**, 083046 (2013).
[43] W. P. Su, J. R. Schrieffer, and A. J. Heeger, *Solitons in polyacetylene*, Phys. Rev. Lett. **42**, 1698 (1979).
[44] A. Blanco-Redondo, I. Andonegui, M. J. Collins, G. Harari, Y. Lumer, M. C. Rechtsman, B. J. Eggleton, and M. Segev, *Topological optical waveguiding in silicon and the transition between topological and trivial defect states*, Phys. Rev. Lett. **116**, 163901 (2016).
[45] J. K. Asbóth, L. Oroszlány, and A. Pályi, *A Short Course on Topological Insulators* (Springer, New York, 2016), Vol. 919.
[46] P. St-Jean, V. Goblot, E. Galopin, A. Lemaître, T. Ozawa, L. Le Gratiet, I. Sagnes, J. Bloch, and A. Amo, *Lasing in topological edge states of a one-dimensional lattice*, Nat. Photonics **11**, 651 (2017).
[47] C. P. Dietrich, A. Fiore, M. G. Thompson, M. Kamp, and S. Höfling, GaAs *integrated quantum photonics: Towards compact and multi-functional quantum photonic integrated circuits*, Laser Photonics Rev. **10**, 870 (2016).
[48] A. S. Helmy, P. Abolghasem, J. Stewart Aitchison, B. J. Bijlani, J. Han, B. M. Holmes, D. C. Hutchings, U. Younis, and S. J. Wagner, *Recent advances in phase matching of second-order nonlinearities in monolithic semiconductor waveguides*, Laser Photonics Rev. **5**, 272 (2011).
[49] R. Horn, P. Abolghasem, B. J. Bijlani, D. Kang, A. S. Helmy, and G. Weihs, *Monolithic source of photon pairs*, Phys. Rev. Lett. **108**, 153605 (2012).

[50] F. Baboux, G. Moody, and S. Ducci, *Nonlinear integrated quantum photonics with* AlGaAs, Optica **10**, 917 (2023).
[51] J. B. Spring, P. L. Mennea, B. J. Metcalf, P. C. Humphreys, J. C. Gates, H. L. Rogers, C. Söller, B. J. Smith, W. S. Kolthammer, P. G. Smith *et al.*, *Chip-based array of near-identical, pure, heralded single-photon sources*, Optica **4**, 90 (2017).
[52] D. J. Brod, E. F. Galvão, A. Crespi, R. Osellame, N. Spagnolo, and F. Sciarrino, *Photonic implementation of boson sampling: A review*, Adv. Photonics **1**, 034001 (2019).
[53] J. Chen, K. F. Lee, and P. Kumar, *Deterministic quantum splitter based on time-reversed Hong-Ou-Mandel interference*, Phys. Rev. A **76**, 031804(R) (2007).
[54] N. Fabre, M. Amanti, F. Baboux, A. Keller, S. Ducci, and P. Milman, *The Hong–Ou–Mandel experiment: From photon indistinguishability to continuous-variable quantum computing*, Eur. Phys. J. D **76**, 196 (2022).
[55] N. Fabre *et al.*, *Producing a delocalized frequency-time Schrödinger-Cat-like state with Hong-Ou-Mandel interferometry*, Phys. Rev. A **102**, 023710 (2020).
[56] O. Meskine, E. Descamps, A. Keller, A. Lemaître, F. Baboux, S. Ducci and P. Milman, *Approaching maximal precision of Hong-Ou-Mandel interferometry with non-perfect visibility*, Phys. Rev. Lett. **132**, 193603 (2024).
[57] M. Scollon and M. P. Kennett, *Persistence of chirality in the Su-Schrieffer-Heeger model in the presence of on-site disorder*, Phys. Rev. B **101**, 144204 (2020).
[58] N. Bergamasco, J. E. Sipe, and M. Liscidini, *Generation of hyper-entangled states in strongly coupled topological defects*, Optics Lett. **46**, 2244 (2021).
[59] A. W. Elshaari, W. Pernice, K. Srinivasan, O. Benson, and V. Zwiller, *Hybrid integrated quantum photonic circuits*, Nat. Photonics **14**, 285 (2020).
[60] L. Yuan, Q. Lin, M. Xiao, and S. Fan, *Synthetic dimension in photonics*, Optica **5**, 1396 (2018).
[61] J. Wang, A. Santamato, P. Jiang, D. Bonneau, E. Engin, J. W. Silverstone, M. Lermer, J. Beetz, M. Kamp, S. Höfling *et al.*, *Gallium arsenide quantum photonic waveguide circuits*, Optics Commun. **327**, 49 (2014).
[62] F. S. Piccioli, A. Szameit, and I. Carusotto, *Topologically protected frequency control of broadband signals in dynamically modulated waveguide arrays*, Phys. Rev. A **105**, 053519 (2022).
[63] X. Wu, L. Wang, G. Li, D. Cheng, D. Yu, Y. Zheng, V. V. Yakovlev, L. Yuan, and X. Chen, *Technologically feasible quasi-edge states and topological Bloch oscillation in the synthetic space*, Opt. Express **30**, 24924 (2022).